Copyright

by

Young-Soo Sohn

2001

MEMS BASED MICROFLUIDIC STRUCTURE FOR BIOLOGICAL AND CHEMICAL SENSOR ARRAY

by Young-Soo Sohn, B.S., M.S.

DISSERTATION

Presented to the Faculty of the Graduate School of
The University of Texas at Austin
in Partial Fulfillment
of the Requirements
for the Degree of

DOCTOR OF PHILOSOPHY

The University of Texas at Austin
May 2001
MEMS BASED MICROFLUIDIC STRUCTURE FOR BIOLOGICAL AND
CHEMICAL SENSOR ARRAY

Approved by Dissertation Committee:

Dean P. Neikirk, Supervisor Jack C. Lee Carlton G. Willson John T. McDevitt Ray T.Chen

ACKNOWLEDGMENTS

I would like to thank my advisor, Professor Dean P. Neikirk, for his guidance over the years I spent as a member of Micro Electromagnetic Device Group. Especially, without his patients and supports during this research, it is impossible for me to finish this work. I am happy to work with Professor John T. McDevitt, Prof. Eric V. Anslyn, and Prof. Jason B. Shear about Electronic Tongue project. Also, I would like to thank Prof. C. Grant Willson for giving me valuable suggestions. To my other committee members, Prof. Jack C. Lee and Prof. Ray T. Chen, I also would like to express my appreciation for their time and interest on this work.

I would like to thank members of group for their friendship. I want to express my special thanks to my former member, Rob Friar, for his friendship and valuable discussion.

Finally, I would like to thank to my parents for their help.

MEMS BASED MICROFLUIDIC STRUCTURE FOR BIOLOGICAL AND CHEMICAL SENSOR ARRAY

Publication	No.

Young-Soo Sohn, Ph.D.

The University of Texas at Austin, 2001

Supervisor: Dean P. Neikirk

A micromachined fluidic sensor array has been developed for the rapid characterization of multiple analytes in solution. A simple micromachined fluidic structure for this chemical and biological detection system has been designed and fabricated, and its operational characteristics have been investigated. Sensing occurs via optical changes to indicator molecules (receptors) that are attached to polymeric microspheres (beads). A separate optical detector, typically a charged-coupled-device (CCD), is used for the simultaneous acquisition of the optical data from selectively arranged beads in micromachined cavities. The fluidic structure for supporting the beads has been designed to be compatible with this hybrid optical detection system. The structure consists of three layers: cover glass,

micromachined silicon, and glass substrate. The fabrication has been ordered to protect receptors that may be changed in their characteristics during the fabrication. The bottom two layers, micromachined silicon and glass substrate, are fabricated first, and the beads are selectively placed into micromachined cavities. Then, cover glass is applied to confine the beads. This structure utilizes surface tension force to draw a liquid sample into the sensor array without moving components, producing a compact, portable, and potentially low-cost device. The fluid flow has been observed using test structures and beads that are sensitive to the sample fluid, allowing time domain characterization of the fluid flow. The test results show that this system may be useful in a micro total analysis system (m-TAS), especially in disposable biomedical applications.

Table of Contents

List of Tables	ix
List of Figures	X
Chapter 1 Introduction	1
Chapter 2 Review of Chemical Sensors and MEMS	6
2.1 Chemical Sensors	6
2.2 MEMS	8
2.3 MEMS Fabrication Techniques	10
2.3.1 Bulk Micromachining	12
2.3.1.1 Isotropic wet etching	13
2.3.1.2 Anisotropic wet etching	13
2.3.2 Surface Micromachining	15
2.3.3 LIGA	19
2.3.4 Bonding	19
2.3.4.1 Anodic bonding	20
2.4 Summary	22
Chapter 3 Device Design	24
3.1 Basic Sensing Scheme	24
3.2 Requirements and Constraints	27
3.3 Device Design	29
3.4 Evolution of Structure	33

3.5 Summary	35
Chapter 4 Fabrication of Microfluidic Structure	36
4.1 Fabrication of Silicon	36
4.2 Bonding of Glass Substrate and Micromachined Silicon	45
4.3 Placing Beads	49
4.4 Applying Cover Glass	51
4.5 Summary	52
Chapter 5 Results and Discussions	54
5.1 Contact Angle	54
5.2 Channel Openings	58
5.3 Fluid Flow	68
5.4 Observation of Bottom Channel	72
5.5 Time Domain Characterization of Fluid Flow	76
5.6 Swelling of Bead	98
5.7 Summary	107
Chapter 6 Conclusion	108
Bibliography	112
Vita	124

List of Tables

Table 2.1: Properties of silicon compared with other materials	12
Table 2.2: Comparison between bulk and surface micromachining	16
Table 2.3: Combination of structural and sacrificial layers in surface	
micromachining	17
Table 4.1: Properties of BOROFLOATTM flat glass	46

List of Figures

Figure 2.1:	Schematic diagram of MEMS fabrication techniques	11	
Figure 2.2:	Figure 2.2: Pyramid pit bounded by silicon (111) crystallographic planes when		
exposed to an	anisotropic etchant	15	
Figure 2.3:	Surface micromachining: (a) patterned sacrificial layer; (b)		
patterned struc	etural layer; (c) suspended structure after sacrificial etching	18	
Figure 2.4:	A schematic diagram of an experimental set-up for anodic bo	onding	
	21		
Figure 3.1:	A simplified hybrid optical detection system	25	
Figure 3.2:	The data analysis system	26	
Figure 3.3:	The change of size of the beads: (a) dry state of beads; (b) sw	ollen	
of beads in aqueous media. 28			
Figure 3.4:	A cross sectional view of the microfluidic structure	31	
Figure 3.5: Top and bottom views of the microfluidic structure: (a) top view;		iew;	
(b) bottom view 33		32	
Figure 3.6:	The so-called 'zero's generation of the microfluidic structure	34	
Figure 4.1:	Schematic view of fabrication procedure of an array of		
micromachined cavities: (a) deposition of mask layer (Si3N4); (b) pattern for			
array of etch c	avities; (c) etching of silicon by KOH solution	37	
Figure 4.2:	A micromachined cavity and a bead: (a) pyramid pit formed	by	
micromachinii	micromachining; (b) micromachined cavity and a bead 41		

Figure 4.3:	Schematic view of fabrication procedure of the channels and	
deposition of silicon dioxide layer: (a) patterns for the channels on both sides; (b)		
etching for the channels on both sides; (c) removal of the mask layer and		
deposition of s	silicon dioxide (SiO2) layer	42
Figure 4.4:	Etch rates of (100) planes of silicon by KOH 45 % at 70 °C	43
Figure 4.5:	Top and bottom views of the micromachined device: (a) top	view;
(b) bottom view		44
Figure 4.6:	A graph of current density verses time of anodic bonding	47
Figure 4.7:	Schematic view of fabrication procedure of coupling the glas	ses
and placing the beads: (a) attachment to glass substrate by bonding; (b) placement		
of the beads in the etch cavities; (c) applying cover glass 48		
Figure 4.8:	An apparatus for picking and placing beads	50
Figure 4.9:	Top view of the device with the beads in the micromachined	
cavities	51	
Figure 4.10:	The fully fabricated microfluidic device	52
Figure 5.1:	Contact angle (q) effects at liquid-gas-solid interface	56
Figure 5.2:	Contact angles at DI-water, air, surface interfaces: (a) silicon	; (b)
silicon nitride;	; (c) silicon dioxide	57
Figure 5.3:	A cross sectional view of the microfluidic structure with deno	oting
top channel opening		

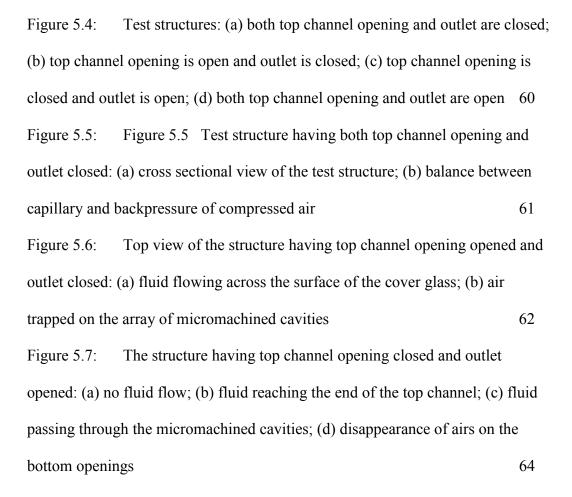


Figure 5.8: Structure having both openings on top and bottom channels opened: (a) no fluid flow; (b) fluid flowing on the array; (c) fluid reaching the end of the top channel; (d) fluid starting to pass through the micromachined cavities; (e) airs on the bottom openings; (f) disappearance of airs on the bottom openings

66

Figure 5.9:	Bottom channel of 250 mm thick silicon substrate: (a) no flui	d	
going through the bottom openings; (b) fluid going through the bottom openings;			
(c) fluid filling the bottom channel. 74			
Figure 5.10:	Bottom channel of 275 mm thick silicon substrate: (a) no flui	d; (b)	
fluid starting t	to reach the bottom openings; (c) evaporation of fluid at the bo	ttom	
openings	75		
Figure 5.11:	The configuration of the beads in the array	77	
Figure 5.12:	Size distribution of the beads in array	78	
Figure 5.13:	igure 5.13: Location and disappearance of bubbles (4 samples) with time 79		
Figure 5.14:	Intensities of an alizarin bead in pH 1 HCl solution	80	
Figure 5.15:	Initial reaction times of the beads in array	81	
Figure 5.16:	Initial reaction time verses diameters of the beads	82	
Figure 5.17:	Two sequent movie frame to define bubble disappearance tin	ne of	
target bead ($t = 8.67 \text{ sec.}$): (a) $t = 8.56 \text{ sec}$; (b) $t = 8.67 \text{ sec}$			
Figure 5.18:	Distribution of bubble disappearance time	84	
Figure 5.19:	Initial reaction time verses bubble disappearance time	85	
Figure 5.20:	(a) Distribution of saturation time of red intensity; (b) distribution	ution	
of saturation time of green intensity; (c) distribution of saturation time of blue			
intensity	88		

Figure 5.21:	(a) Diameters of the beads verses saturation time (red); (b)		
diameters of the beads verses saturation time (green); (c) diameters of the beads			
verses saturation time (blue) 91			
Figure 5.22: Another configuration of alizarin and blank beads in			
micromachined cavities 94			
Figure 5.23:	ure 5.23: The distribution of initial reaction time of the beads in the array		
	95		
Figure 5.24:	The size distribution of the beads in the array	96	
Figure 5.25:	A graph of initial reaction time verses the size of the beads	97	
Figure 5.26: Time sequent movie frames assuming DI-water diffuses into the		the	
alizarin bead: (a) $t = 30 \text{ sec}$; (b) $t = 35 \text{ sec}$; (c) $t = 38 \text{ sec}$			